Current Science International
ISSN: 2077-4435

Volume : 06 | Issue : 01 | Jan.- Mar. |2017
Pages: 58-74

Synthesis of $CuAl_2O_4$ Nanoparticles and Its Application Towards Adsorptive Removal of Hazard Dye Chicago Sky Blue from Wastewater

Saleh D. Mekkey

Department of Chemistry, Faculty of Science, Al-Azhar University, Cairo, Egypt.

Received: 30 November 2016 / Accepted: 07 January 2017 / Publication date: 15 January 2017

ABSTRACT

The present study focused on the synthesis of mixed oxide Cu–Al via a modifying Pechini method and applied for the adsorptive removal of carcinogenic dye Chicago sky blue (CSB) in water. The synthesized Cu–Al spinel nanoparticles were characterized by FTIR, XRD and SEM with an attached EDX and a BET surface area Analyzer. Batch adsorption experiments were conducted to evaluate the adsorption process by varying the solution temperatures (304, 310, 318 and 326 K). The process was initially very rapid, and the maximum adsorption was observed within 60 min of contact time. The kinetics of removal were tested with a pseudo-first order, a pseudo-second order, Elovich, film and an intra-particle diffusion models and showed the best agreement with the pseudo-second order model. Adsorption data were modelled with Freundlich, Langmuir, Temkin, and Dubinin–Radushkevich (D-R) isotherms and had a good fit with the Langmuir isotherm model. The adsorption process was endothermic with positive values of ΔH of 55.11 kJ/mol and was spontaneous, as the ΔG value was negative for all of the temperatures. A positive ΔS value indicates increased disorder at the solid–solution interface during the adsorption of the CSB dye. The successful removal of CSB from the studied water samples indicates that the mixed oxide Cu–Al nanoparticle can be used efficiently for pollution remediation of fresh water from Chicago sky blue.

Key words: $CuAl_2O_4$; CSB dye; Removal; Kinetics; Thermodynamic

Introduction

The release of coloured wastewater into nearby bodies of water brings about great harm to aquatic animals and plants because the dyes and their by-products alter the water chemistry. Coloured wastewater interferes with the transmission of sunlight into streams and reduces photosynthetic activity (Roosta *et al*., 2012), which results in the gradual destruction and disruption of aquatic ecosystems (Gautam *et al*., 2013). Moreover, dyes can cause severe health disorders in human beings and affect the function of kidneys, the reproductive system, the liver, the brain, and the central nervous system and might be carcinogenic, mutagenic, or allergenic to aquatic life (Duran *et al*., 2011). Hence, an urgent need to treat dye-containing wastewater effluents prior to discharge into nearby bodies of water exists. Nowadays, more than one hundred thousand kinds of commercial dyes are used in the production of over 9 million tons annually (Mayur *et al*., 2017). Therefore, improving a sustainable method for the removal of colour from effluents containing various kinds of synthetic dyes has long been a challenge for scientists. In particular, many efforts have been made to develop different kinds of materials to remove dyes from drinking water.

Different methods have been used for dye removal from wastewaters such as biological degradation (Fan *et al*., 2017), photocatalytic degradation (Lin *et al*., 2017), coagulation (Xin *et al*., 2017a), membrane filtration (Bouazizi *et al*., 2017), reverse osmosis (Yue *et al*., 2017), ozone treatment (Mena *et al*., 2017), adsorption (Muhammad *et al*., 2017), or the synergy treatment using different methods. Among these methods, the adsorption process is one of the most effective techniques that has been successfully employed for colour removal because it is considered to be less expensive, more efficient and less likely to generate secondary waste (Zhenzhen *et al*., 2017). Most conventional adsorption systems use activated carbon despite its high production costs and regeneration difficulty. As one alternate effective process, adsorption technology has been regarded as one of the most promising and widely used methods due to its effectiveness, efficiency, economy and

Corresponding Author: Saleh D. Mekkey, Department of Chemistry, Faculty of Science, Al-Azhar University, Cairo, Egypt.
E-mail: salehsdmm@yahoo.com

no secondary pollution. A number of materials, including metal oxides and hydroxides (Sneha *et al*., 2017; Wei *et al*., 2017), agricultural wastes (Thines *et al*., 2017), clays (Dordio *et al*., 2017), Chitosan (Agnès *et al*., 2017), silica (Zhijie *et al*., 2017), kaolinite (Xin *et al*., 2017b), sepiolite (Sílvia *et al*., 2016), graphene oxide (Yunchuan *et al*., 2017), active carbon (Somayeh *et al*., 2017), montmorillonite (Boran *et al*., 2017), zeolites (Lu *et al*., 2017) and some natural biosorbents (Ying-Lung *et al*., 2017). However, these materials generally have low adsorption capacities, and hence, a large adsorbent dosage is required to achieve a low dye concentration in the treated effluents.

Many of the authors reported that calcination markedly improved the solute uptake by layered double hydroxides LDHs (Wei *et al*., 2017; Chunsheng *et al*. 2017). The improvement was extensively explained by the dehydration of the calcined LDHs in water, "memory effect", and the increased specific surface area after calcination. However, the mechanisms of the adsorption process onto calcined LDHs, are still not clear.

Chicago sky blue, also known as Niagara sky blue, is a vital dye that can successfully be used as an intravascular energy absorbing target for the light from a helium-neon laser. The result of this light/dye interaction is endothelium damage which can be controlled by adjusting the duration of the laser exposure and the amount of dye injected intravenously. The endothelial damage probably is the result of the heat generated by the dye absorption of energy at the interface between plasma and endothelium. The most minimal damage resulted in selective loss of the dilation normally produced by acetylcholine and bradykinin, two endothelium dependent dilators. The dilation produced by sodium nitroprusside, a dilator acting directly on vascular smooth muscle, was preserved. More severe injury, i.e. more prolonged exposure to light and/or more dye, resulted in local platelet aggregation at the site of laser impact (Nishimura *et al*., 1989).

In the present work, copper, aluminium-mixed oxide was synthesised via a modifying Pechini method and used as an adsorbent of Chicago Sky Blue dye (CSB) after calcination at 800^0C. The sample was characterised by powder XRD, FTIR, SEM and EDX. The effects of various parameters such as contact time and temperature on the removal of Chicago Sky Blue dye by this precursor were studied in detail. The adsorption kinetic data were tested by pseudo-first-order, pseudo-second-order and intraparticle diffusion kinetic models. The equilibrium data were analysed using the Langmuir, Freundlich, Temkin and Dubinin–Radushkevich (D-R) isotherm models. Thermodynamic parameters were also evaluated at three different temperatures.

Experimental details:

Chemicals and reagents:

All of the reagents were of analytical grade with the mass fraction purity of 0.99 and used as received without further purification. $AlCl_3$, Cupric chloride, citric acid, Ethylene glycol were purchased from British Drug House, Poole, England. The anionic sulfonated azobenzene dye used in these experiments is Chicago Sky Blue 6B (CSB). CSB (Molecular weight 992.82, purity >99%) were purchased from Aldrich Chemical Co., USA and handled using proper safety procedures. It was used without further purification. Chicago Sky Blue 6B stock solutions (1000 mg /l) was prepared by dissolving the required amount in double distilled water and the working solution was prepared daily with the required dilution.

Chicago Sky Blue 6B (CSB) with IUPAC names of sodium 4-[(4-dimethylamino) phenyldiazenyl] benzene sulfonate (Fig.1) is a typical water-soluble anionic.

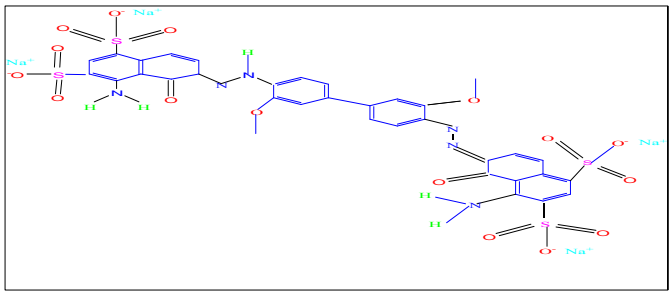

Fig. 1: Chicago Sky Blue B6 dye

Powder preparation:

$CuAl_2O_4$ nanoparticle was prepared in briefly as the following (Fig.2), aluminium chloride [$AlCl_3$] and Cupric chloride [$CuCl_2.2H_2O$] were dissolved in distilled water and citric acid (CA) was then added (molar ratio CA: total cations = 1). The mixture was magnetically stirred until a clear yellowish solution was obtained. Ethylene glycol (EG, M.Wt = 62.07) was added to this solution in the molar ratio EG:CA = 2. The solution was continuously stirred at around 80 °C in order to facilitate the evaporation of the excess water and accelerate the polyesterification reaction. During the polyesterification process no turbidity or precipitation was observed. The procedure was stopped when a viscous gel was obtained. The gel was then heated at 150 °C in an oven for 24 h. The xerogel was ground and calcined at 800 °C for 6 h to obtain the $CuAl_2O_4$ nanoparticle.

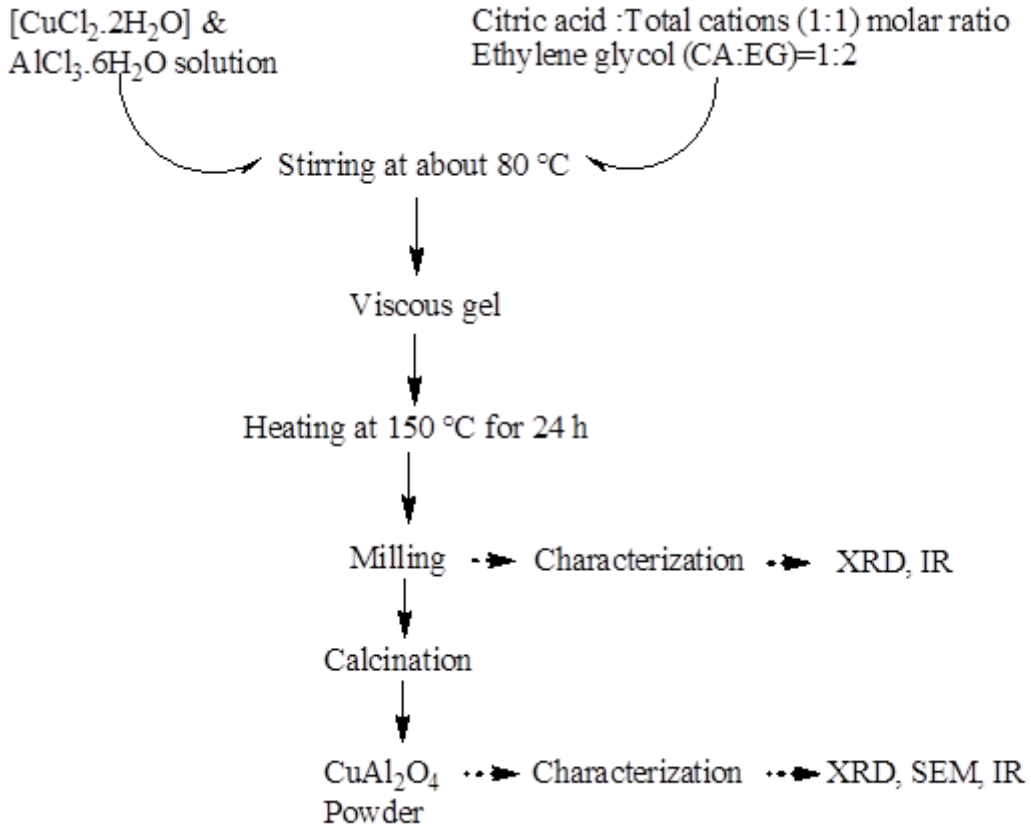

Fig. 2: Flow chart of the $CuAl_2O_4$ preparation process

Characterization of $CuAl_2O_4$ nanoparticle:

The prepared product was characterized using X-ray diffraction (XRD), scanning electron microscopy (SEM), energy dispersive X-ray analysis (EDAX), surface area determination using BET analysis and FTIR analysis. Scanning electron microscope (SEM) analysis was performed with a Quanta 250 FEG (Field Emission Gun) attached with EDX Unit (Energy Dispersive X-ray Analyses), with accelerating voltage 30 K.V., magnification14x up to 1000000 and resolutions for Gun.1n). Infrared spectrum (IR) was obtained using a JASCO 6100, made in Japan infrared spectrometer. X-ray diffraction (XRD) pattern was measured at room temperature by using a Philips diffractometer (type PW-3710). The patterns were run with Ni-filtered copper radiation (θ = 1.5404 Å) at 30 kV and10 mA with a scanning speed of 2θ = 2.5◦/min. The mean particle size was calculated using the Debye–Scherrer Eq. [(Kλ)/(βcosΘ)], in which K is a constant equal 0.9, λ is the wavelength of the Cu Kα radiation, β is the half peak width of the diffraction peak in radiant.

Adsorption experiments:

The adsorption of dyes was carried out in the dark to avoid photolysis of Chicago Sky Blue (CSB) at the natural pH. Natural pH was measured in aqueous media without any addition of external ions. A stock solution of 200 ppm was prepared and kept in the dark. This was used for adsorption studies after appropriate dilution. The amount of adsorbent was kept constant at 0.2 g/100 ml unless otherwise mentioned. The solution was continuously stirred at 400–500 rpm to maintain homogeneity throughout the solution. The effect of contact time (0–240 min) and various temperatures on the adsorption performance at constant 0.2 g $CuAl_2O_4$ nanoparticle and initial CSB concentration of 68 mg/L were investigated.

The samples were taken out at suitable intervals for the measurement of concentration of dye in liquid phase. The aliquots were centrifuged to remove the adsorbent particles and the absorbance was measured using UV–vis spectrophotometer (UV 1700, Shimadzu, Japan) at the characteristic wavelength (λ) of the dye (CR-497 nm, OG-480 nm, IC-610 nm, MB-600 nm). The calibration based on Beer Lambert's law was used to convert absorbance to concentration. The absorbance varied proportionally with dye concentration as absorbance = A × concentration. The values of A were varied for CSB, and this calibration is valid up to dye concentration of 68 mg/l. For higher concentrations, dilution was carried out and accordingly the concentration was obtained by multiplying by the dilution factor.

The adsorption capacity and removal ratio of adsorbent can be calculated according to the Eqs. (1) and (2), respectively:

$$q_t = \frac{(C_0 - C_e)\,v}{m} \quad (1)$$

$$R = \frac{Co - Ce}{Co} x100 \quad (2)$$

where q_t is the adsorption capacity at the time t, mg/g; C_0 and C_e are the initial and equilibrium concentration of (CSB), mg/L; R is the removal ratio, %; V is the volume of solution, L and m is the dose of adsorbent sample, g.

Results and Discussion

Characterization of the adsorbent

The mixed oxide $CuAl_2O_4$ nanoparticle was further characterized by FTIR analysis. Fig. 3. Fig. 3 shows the FT-IR spectra of the calcined product. From this Figure, the bands at 3500 cm^{-1} and 1384 cm^{-1} are not present in the calcined sample, which are attributed to the removal of water molecules and the decomposition of the NO_3^- groups in the mixed oxide $CuAl_2O_4$ interlayer. In the calcined sample, the bands at 536 and 593 cm^{-1} are related to Al─O bonds in the $CuAl_2O_4$ phase (Ahmed *et al*., 2012; Xiaoyun *et al*., 2012). The band at 709 cm^{-1} are assigned to the stretching modes of AlO_6 octahedral units, and the band observed at 536 cm^{-1} is due to the bending mode of AlO_6 octahedral units (Silva *et al*., 2009; Mei-Yu *et al*., 2013).

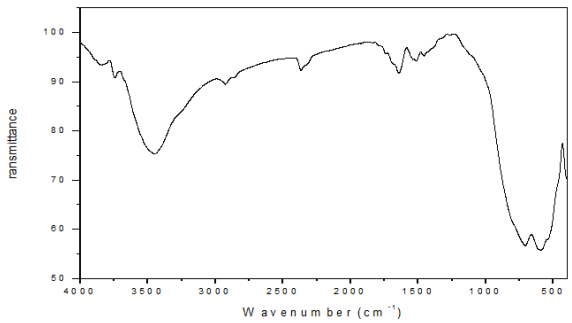

Fig. 3: FTIR plot of the adsorbent ($CuAl_2O_4$)

Morphology of the $CuAl_2O_4$ nanostructures was investigated with SEM as shown in Fig. 4. The prepared nanosized particles are well dispersed and similarly spherical. The corresponding particle size distribution (inset in Fig. 4) indicates the average diameter of $CuAl_2O_4$ is about 24.12 nm. The

EDAX is shown in Fig. 5. The results show that the mixture is uniform as the image shown and the atomic % of aluminium is around 2 times of that of copper. This confirms the formation of $CuAl_2O_4$.

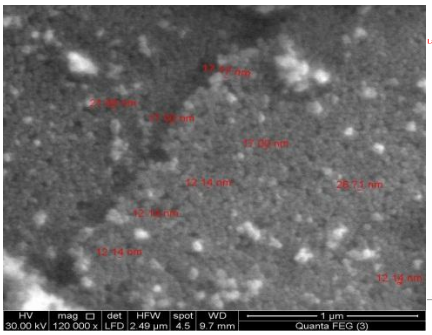

Fig. 4: SEM of the adsorbent

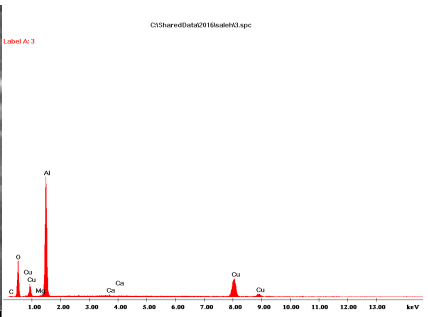

Fig. 5: EDAX of the adsorbent

The XRD patterns for $CuAl_2O_4$ are shown in Fig. 6. All the diffraction peaks can be perfectly indexed to face-centred cubic spinel-structured $CuAl_2O_4$. The diffraction peaks of the produced powders and that of standard were the same. This indicates that there is a complete formation of the spinel phase in all the samples synthesized in the experimental conditions employed in this work. No impurities were detected in the samples synthesized.

Nitrogen adsorption–desorption isotherms for the $CuAl_2O_4$ sample prepared is displayed in Fig. 7. According to IUPAC classification, the isotherms for samples are of type IV, representing predominantly mesoporous structure characteristics. The mesoporous structure was confirmed by the analysis of pore size distribution, which shows the spectra of the pore diameter with the defined maxima in the mesoporous region of the sample. The pore size distribution curve displays a wide unimodal distribution with an average pore size ranged from 13.87 to 34 .36 nm for the sample. In addition, the total pore volume was 0.0635 cc/g. The value of the BET surface area is also determined. The sample obtained by the co-precipitation method had a relatively small area at approx. 79.24 $m^2\ g^{-1}$. These features are of great importance for the adsorption purposes because it allows for a greater accessibility of reactant molecules to the oxide material.

The average crystallite size was estimated by applying the Scherrer formula on the highest intensity peak for each sample. An average size of around 10–20 nm was obtained for the sample. Therefore, XRD results provide further support for the formation of a $CuAl_2O_4$ spinel during calcination, which is in good agreement with FT-IR spectra.

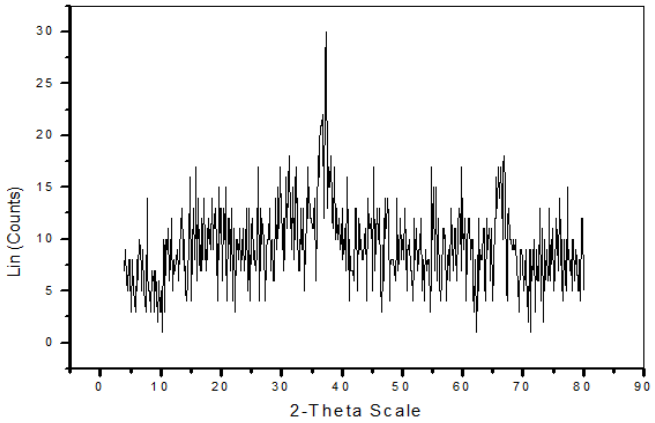

Fig. 6: XRD plot of $CuAl_2O_4$ adsorbent

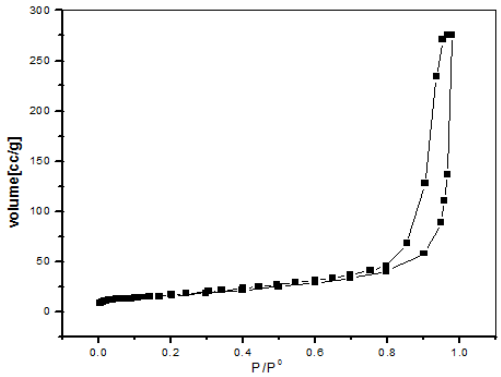

Fig. 7: BET plot of the adsorbent

Effect of temperature:

Effect of temperature on the CSB dye removal was studied in the range of 304 to 326K while keeping all other parameters constant. The results explored in Fig.8, indicate that the adsorption rate increases with an increase in temperature, and indicate that the process is apparently endothermic and governed by chemical forces. This may also be the result of the decreased desorption process of an increase in thermal energy of the adsorbate. On the other hand, the removal percentage of CSB onto the $CuAl_2O_4$ nanoparticle (Fig.8) was increased with increase of temperatures ranged from 88.97 to 97.35% by the $CuAl_2O_4$ nanoparticle, with increase in temperature from 304 to 326 K. This may be due to the formation of new active sites in the adsorbent to increase in temperature, activation of the adsorbing surface and increase in the mobility of CSB dye. Also, this fact demonstrated an endothermic sorption process (Shuheng *et al*., 2016; Xiang *et al*., 2017). On the other hand, the time-dependent adsorption of target dye onto the adsorbent was investigated at four different temperatures namely, 304, 310, 318 and 326K and a constant dye concentration of 68 mg/l. The results shown in Fig. 8 indicated that the dye was rapidly adsorbed by the adsorbent at the initial 60 min. Decreasing of adsorption rate after 60 min may be attributed to the lack of active sites on the adsorbent and the increasing repulsive forces between the anionic dyes on the solid and in the bulk phases. However, the adsorption equilibrium time was decreased with increasing the dye solution temperature, namely, 304, 310, 318 and 326 K and reached gradually within 360, 330, 300 and 200 min, demonstrating the strong affinity of the adsorbent towards anionic dyes as well as the fast mass transfer of absorbent as the temperature increased.

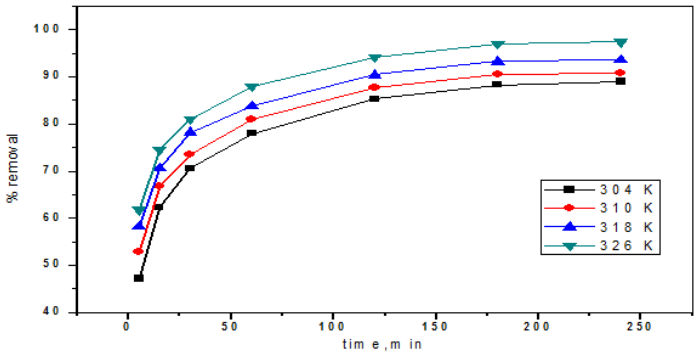

Fig. 8: Effect of temperature on the % removal of CSB

Bright colour of an aqueous solution of the CSB dye could be clearly observed in the Fig. 9, but after raising the temperature 304 to 326K, the colour of the solution significantly faded. Change of the dye colour solution was another supporting factor indicating the fact that, an increasing solution temperature has a high effect on the removal process.

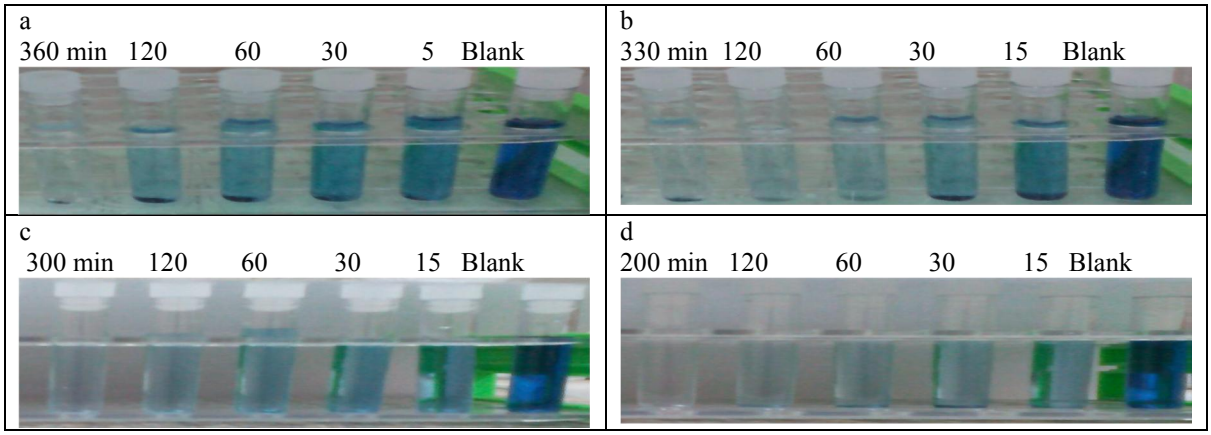

Fig. 9: Effect of temperature on CSB dye colors at (a) 304K, (b) 310K, (c) 318K and (d) 326K

The distribution ratio (D):

Distribution ratio D for CSB was determined by the batch method at different temperature systems (304, 310, 318 and 326K). The distribution ratio, D, is defined as the ratio of the adsorbate concentration on the adsorbent to that in the aqueous solution and can be used as a valuable tool to study CSB mobility. The distribution ratio D is defined by the following relationship:

$$K_d = qe/Ce \quad (3)$$

Fig. 10 shows that the distribution ratio (D) values decrease with the increase in temperatures of dye solutions. A corresponding increase in the distribution ratio (K_d) with the increase in temperature of the sorbate solution was observed, illustrating that at higher temperatures of the sorbate, higher number of sorption sites are available onto sorbent surface and the study is in agreement with earlier reported work (Xiaoming *et al*., 2016). The rapid CSB sorption has significant practical importance, as this will facilitate with the small amount of adsorbent to ensure efficiency and economy.

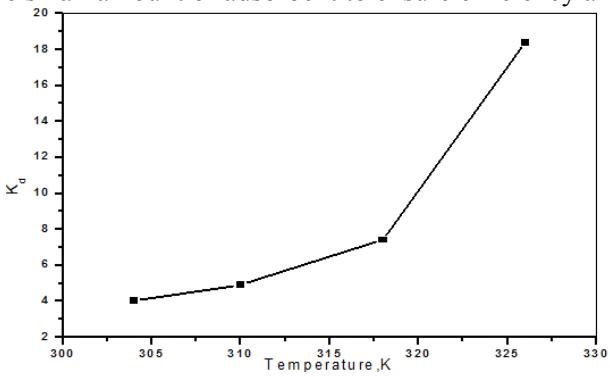

Fig. 10: The distribution coefficients of CSB adsorption

Adsorption isotherms:

To better describe the adsorption properties of anionic dyes by $CuAl_2O_4$ nanoparticle, the adsorption isotherm for CSB dye was investigated at 100 ml dye solution of 68 mg/l, 0.2 g $CuAl_2O_4$ nanoparticle and over the temperature dye solution range of 304–316K. Four well-known types of isotherm models, Freundlich 1906, Langmuir 1918, Temkin 1940 and Dubinin Redushkevich 1947 were used to fit the equilibrium data.

The Freundlich model is an empirical equation used to characterize heterogeneity of the adsorbents (Ahmad *et al*., 2017). Whereas the Langmuir model is based on the assumption that one active site can only be occupied by one adsorbate molecule and all the adsorption sites are energetically identical (Tomić *et al*., 2014), thus, a monolayer adsorption process takes place on the homogeneous adsorbent surface.

The Freundlich equation (Eq. 4) and the Langmuir equation (Eqs. 5) could be represented as follows:

$$q_e = K_F C_e^{1/n} \quad (4)$$

$$q_e = Q_{max} K_L C_e/(1+K_L C_e) \quad (5)$$

where q_e (mg g^{-1}) is the amount of the dyes adsorbed at equilibrium, C_e (mg l^{-1}) is the equilibrium concentration of the dyes in solution. K_F (mg g^{-1} (l $mg^{-1})^{1/n}$) and n are the Freundlich constants related to the adsorption capacity and intensity, respectively. Generally, the values of 1/n are between 0 and 1. The 1/n value close to 1 (Fig.11) indicates that the adsorbent has a more homogeneous surface (Alpat *et al*., 2008). Q_{max} (mg g^{-1}) is the maximum monolayer adsorption capacity and K_L (l mg^{-1}) represents the Langmuir constant reflecting the adsorption energy.

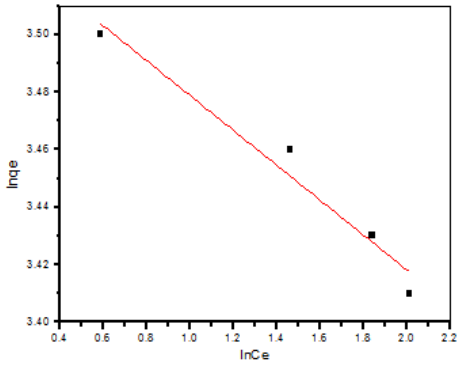

Fig. 11: Freundlich plot of CSB adsorption

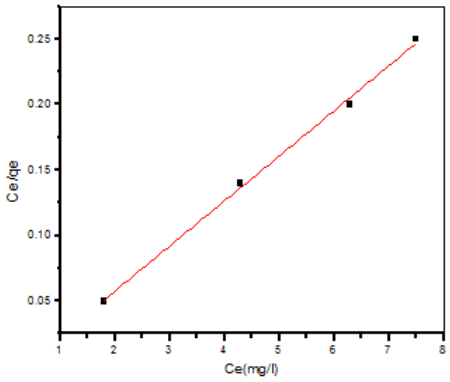

Fig. 12: Langmuir plot of CSB adsorption

The fittings of the isotherms were displayed in Figs. 11,12 and the corresponding parameters were summarized in Table 1. As is shown, the Langmuir model with much higher value of R^2 (0.99649) could better fit the equilibrium data, suggesting the monolayer coverage of the target dye on the surface of $CuAl_2O_4$ nanoparticle (Jianguo *et al*., 2016; Long *et al*., 2017; Xi *et al*., 2017).

Furthermore, a dimensionless constant separation factor (R_L) was used to explain the essential characteristics of Langmuir isotherm. And the R_L is defined as follows:

$$R_L = 1/(1+ K_L C_0) \quad (6)$$

where K_L and C_0 have already been explained above. Thus, R_L is a positive value whose magnitude determines the feasibility of the adsorption process. As indicated in Table 1, the values of R_L were between 0 and 1, suggesting the favourable adsorption of CSB as an anionic dye by the mixed oxide $CuAl_2O_4$ nanoparticle.

The Temkin isotherm contains a factor that explicitly taking into the account of adsorbent–adsorbate interactions. By ignoring the extremely low and large value of concentrations, this model assumes a uniform distribution of binding energies between the molecules adsorbed and adsorbent.

Plotting the amount adsorbed Q_e against ln C_e is possible obtained the constants from the slope and intercept according to the following model:

$$q_e = B_T \ln A_T + B_T \ln C_e \quad (7)$$

where A_T is Temkin isotherm equilibrium binding constant (L g^{-1}) and B is constant related to heat of sorption (J mol^{-1}). From this model (Fig.13), the following values were estimated $A_T = 5.2x10^7$ L g^{-1} and $B_T = 1.9347$ J mol^{-1}, which is an indication of the heat of sorption indicating a physical adsorption process (Banerjee *et al*., 2017).

Table 1: Isotherm models of CSB dye adsorption

Freundlich			Langmiur			
1/n	K_F (mg/g)	R^2	Q_{max} (mg/g)	K_L (L/mg)	R_L	R^2
0.061	34.45	0.94857	29.04	3.03	$4.83x10^{-3}$	0.99649
Temkin			Dubinin Redushkevich (D-R)			
A_T (L/g)	B_T (J/mol)	R^2	β mol^2/J^2	X_m (mg/g)	E (kJ/mol)	R^2
51807925	1.9347	0.94718	$5.67x10^{-8}$	30.63	2.97	0.75502

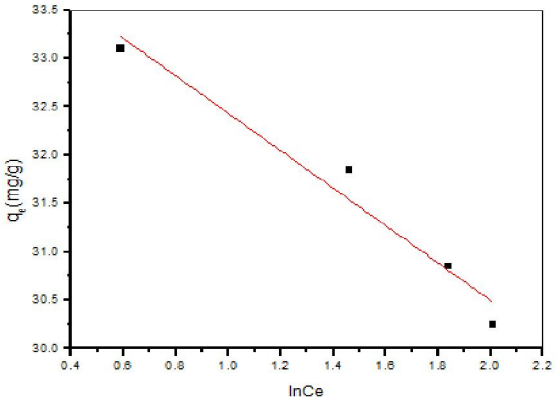

Fig. 13: Temk in plot of CSB adsorption

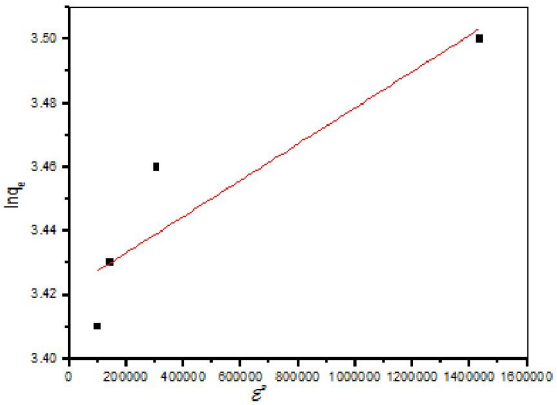

Fig. 14: D-R plot of CSB adsorption

The D–R model is generally used to distinguish between physical and chemical adsorption (Ma *et al*., 2012):

$$\ln q_e = \ln X_m - \beta\varepsilon^2 \quad (8)$$

where q_e is the equilibrium adsorption capacity (mg/g), X_m is the D–R adsorption capacity (mg/g), β (mol^2/kJ^{-2}) is the activity coefficient related to the mean adsorption energy and ε the Polanyi potential given by

$$\varepsilon = RT\ln\left(1+\frac{1}{Ce}\right) \quad (9)$$

where R is the gas constant (8.314 J/mol K) and T is the absolute temperature (K). Thus the plots of ln q_e against ε^2 give a straight line with a slope of β and an intercept of ln X_m (Fig.14). The constant β gives valuable information about the mean free energy E (kJ/mol) of adsorption per molecule of adsorbate when it is transferred to the surface of the solid from infinity in the solution and can be calculated using the following relationship:

$$E = 1/(2\beta)^{1/2} \quad (10)$$

The D–R isotherm constants were calculated and listed in Table 1. The value of E is usually used to estimate the type of adsorption. An ion exchange process has an E value between 8.0 and 16.0 kJ/mol and a physiosorption process has an E value less than 8.0 kJ/mol (Somaye *et al*., 2016). In this study, the values of E were in the range between 0 and 2.97 kJ/mol. This result was consistent with the analysis form D–R adsorption isotherm that the adsorption was physisorption in nature (Arash *et al*., 2017).

Adsorption kinetic model:

The kinetics of adsorption describes the rate of copper ions uptake on ion exchange resins and this rate control the equilibrium time. The kinetics of adsorbate uptake is required for selecting optimum operating conditions for the full-scale batch process. The kinetic parameter, which is helpful for the prediction of adsorption rate, gives important information for designing and modelling the processes. Thus, the effects of initial concentration, contact time, and adsorbent dosage were analysed from the kinetic point of view.

To further study the adsorption process, the pseudo-first-order (Lagergren 1898) and, pseudo-second-order (Ho 1999) kinetics model were applied to fit the experimental data.

The pseudo-first-order model is one of the most widely used equations to describe the adsorption rate based on the adsorption capacity. The linear form is formulated as

$$\ln(q_e - q_t) = \ln q_{e,1} - tk_1 \quad (11)$$

where k_1 is the adsorption rate constant (1/min), q_e and q_t are the amounts of CSB adsorbed at equilibrium and at time t (min). The values of k_1 and $q_{e,1}$ (Table 2) were evaluated from the linear regression of ln($q_e - q_t$) versus t (Fig. 15). The determination coefficient values (R^2) for the pseudo-first-order adsorption model at all temperatures were ranged from 0.9888 to 0.7547. These values were relatively low and the calculated equilibrium adsorption capacities q_e (average 32 mg/g) had a large deviation (51%) compared with the experimental data (68 mg/g). It suggested that the pseudo-first-order model was not suitable to describe the adsorption of CSB onto $CuAl_2O_4$ nanoparticle and the rate-limiting step was not physisorption (Roohan and Yasaman 2017).

The pseudo-second order model is based on the adsorption capacity of the dye molecules on the surface of the adsorbent and its linear form is expressed as follows:

$$\frac{t}{q_t} = \frac{1}{k_2 q_{e,2}^2} + \frac{t}{q_{e,2}} \quad (12)$$

where k_2 (g/(mg min)) is the rate constant of pseudo-second-order adsorption. The values of k_2 and $q_{e,2}$ (Table 2) were calculated from the slope and intercept of the straight portion of the linear plots obtained by plotting t/q_t against t (Fig. 16). The product "h"(mg/g min) = $k_2 q^2_{e,2}$ is the initial adsorption rate. It was reported that if adsorption data followed the pseudo-second order model, the overall rate of the dye adsorption process was controlled by the chemisorption process. The results in Table 2 show that the determination coefficient for the second order kinetic model was very high and ranged from 0.9995 to 0.9980 temperature range of 304 to 326 K. It suggested that the pseudo-second-order model was suitable to describe the adsorption of CSB onto $CuAl_2O_4$ nanoparticle and the rate-limiting step was chemisorption. Similar results have been reported about the adsorption of dyes onto the different adsorbents in the literature (Somayeh *et al*., 2017; Agnès *et al*., 2017; Xin *et al*., 2017c).

The initial adsorption rate ($h = k_2 qe^2$) can be determined from k_2 and q_e values, where k_1 and k_2 are the adsorption rate constants of first and second order kinetic models, in min^{-1} and L $(mg\ min)^{-1}$, respectively; q_e and q_t in mg g^{-1}, are equilibrium adsorption uptake (at time $t = \infty$) and adsorption uptake (at time t), respectively.

As indicated in Table 2, the adsorption of anionic dyes on $CuAl_2O_4$ nanoparticle was considerably better fitted with the pseudo-second-order kinetics model due to the higher values of R^2. Therefore, the pseudo-first-order kinetics was less likely to explain the rate processes. As is known, the electrostatic interaction between protonated amine groups and negatively charged anionic dye is classified into ionic bonds. Moreover, ionic bond involving the electrons sharing between oppositely charged ions is also a type of chemical bonds (Ariel *et al*., 2016). Thus, chemisorption is considered to be the rate controlling step in this study.

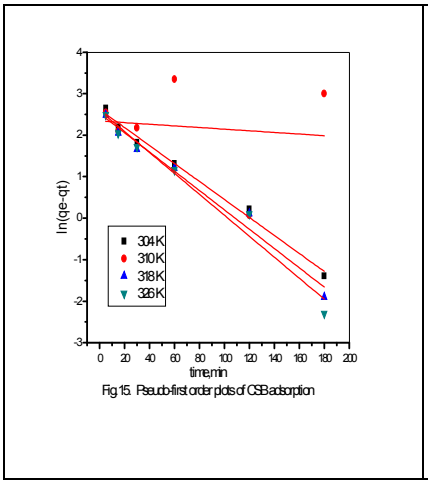

Fig 15. Pseudo-first order plots of CSB adsorption

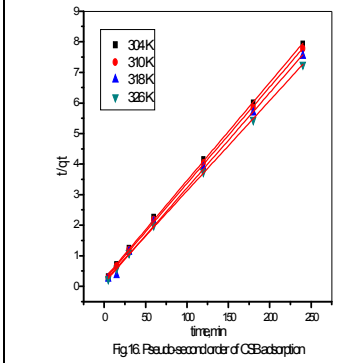

Fig 16. Pseudo-second order of CSB adsorption

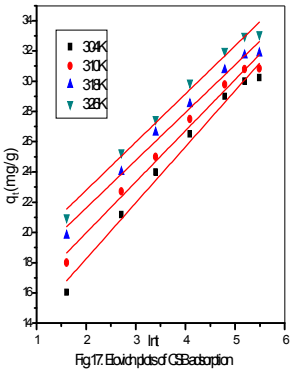

Fig 17. Elovich plots of CSB adsorption

The fitting parameters for the Elovich kinetic models (Robati *et al*., 2015) of CSB adsorption onto the adsorbent at 70 mg/l CSB dye concentration and at different temperatures (Fig. 17) are presented in Table 2.

$$q_t = \frac{1}{\beta}\ln(\alpha\beta) + \frac{1}{\beta} \quad (13)$$

where α is the initial adsorption coefficient ($mg \cdot g^{-1} \cdot min^{-1}$); and β is the desorption coefficient ($g \cdot mg^{-1}$).

Table 2: Kinetic models of CSB dye adsorption

Temp. (K)	The pseudo-first-order			The pseudo-second-order				Elovich model		
	$q_{e,1,cal}$ (mg/g)	K_1 (min^{-1})	R^2	$q_{e,2,cal}$ (mg/g)	K_2 (g/mg min)	h (mg/g min)	R^2	α	β	R^2
304K	13.73	0.02168	0.989	31.14	$4.18x10^{-3}$	4.05	0.999	6.88	0.370	0.984
310K	26.80	0.03044	0.755	31.69	$4.79x10^{-3}$	4.81	0.999	14.79	0.296	0.984
318K	12.54	0.02328	0.976	32.1	$9.41x10^{-3}$	9.69	0.998	40.40	0.317	0.985
326K	13.41	0.02526	0.963	33.83	$5.26x10^{-3}$	6.02	0.999	54.50	0.314	0.986

The Elovich model describes the heterogeneous diffusion process, which is comprehensively regulated by the reaction rate and diffusion factor. The good agreement of the Elovich model with observed results (R^2> 0.98) at the four temperatures studied, namely, 304, 310, 318 and 326 K means that, adsorption of the CSB dye onto $CuAl_2O_4$ adsorbent is a heterogeneous diffusion process and not a simple first-order reaction. The adsorption of CSB onto the adsorbent was an integrative process that was controlled by reaction rate and diffusion, a conclusion that is consistent with the pseudo-second order kinetic model (Shisuo *et al*., 2016).

Adsorption mechanisms:

It is most important to predict the rate-limiting step in an adsorption process to understand the adsorption mechanism associated with the phenomena. For a solid–liquid sorption process, the solute transfer is usually characterized by either external mass transfer (boundary layer diffusion) or intraparticle diffusion or both. The following three steps can describe the adsorption dynamics (Seliem *et al*., 2016; Acharya *et al*., 2009).

1- The movement of adsorbate molecules from the bulk solution to the external surface of the adsorbent (film diffusion).

2- Adsorbate molecules move to the interior part of the adsorbent particles (particle diffusion).

3- Sorption of the solute on the interior surface of the pores and capillary spaces of adsorbent (sorption).

Boyd kinetic model:

The third step in the adsorption dynamics of CSB is assumed to be very rapid and it can be considered negligible. For design purposes, it is required to distinguish between film diffusion and particle diffusion of adsorbate molecules. In order to identify the slowest step in the adsorption process, Boyd kinetic equation (Boyd *et al*., 1947) [39] was applied, which is expressed as:

$$F = 1 - \frac{6}{\pi} \exp(-Bt) \quad (14)$$

$$F = q_t/q_e \quad (15)$$

where q_e is the amount of the dye adsorbed at equilibrium (mg/g) and q_t represents the amount of the dye adsorbed at any time t, F represents the fraction of the dye adsorbed at any time t, and Bt is a mathematical function of F (Reichenberg 1953).

The plot of Bt against time t can be employed to test the linearity of the experimental values. If the plots are linear and pass through the origin, then the slowest step in the adsorption process is the internal diffusion. From Fig. 18, it was observed that the plots are linear, but do not pass through the origin, suggesting that the adsorption process is controlled by film diffusion. The calculated B values were used to calculate the effective diffusion coefficient, D_i (m^2/s) using the following relationship:

$$B = \frac{\pi 2\, Di}{r2} \quad (16)$$

where D_i is the effective diffusion coefficient of CSB in the $CuAl_2O_4$ nanoparticle surface and r is the radius of the resin particles (Table 3). The D_i values were found to be 0.529, 1.029, 0.967 and 0.994 (cm^2/s) at four different temperatures 304, 310, 318 and 326 K, respectively. A Boyd kinetic plot confirms that the external mass transfer was the slowest step involved in the adsorption process.

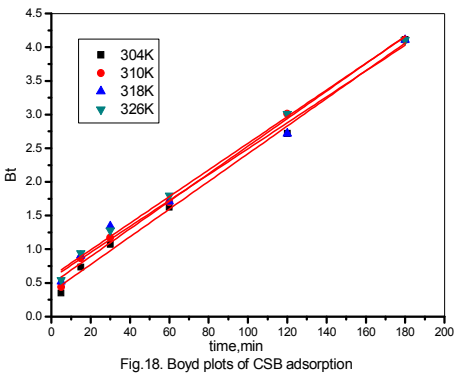

Fig.18. Boyd plots of CSB adsorption

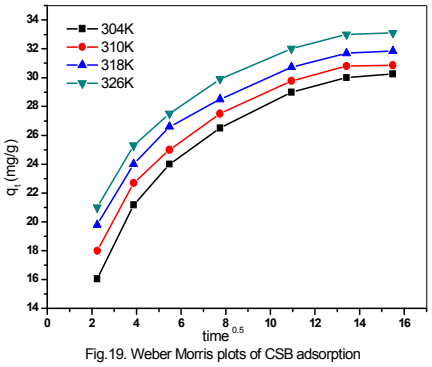

Fig.19. Weber Morris plots of CSB adsorption

The intraparticle diffusion model:

This model is normally used for a deeper understanding of the adsorption mechanism. A plot of q_t versus $t^{0.5}$ should be a straight line when the adsorption process is controlled by the intraparticle diffusion where the adsorbate ions diffuse in the intraparticle pore of the adsorbent. However, more than one step could govern the process if the data exhibit multi-linear plots. The intraparticle diffusion co-efficient, k_{id}, can be determined by fitting the experimental data in the intraparticle diffusion model (Weber and Morris, 1963) expressed as:

$$q_t = k_{id}t^{1/2} + C \quad (17)$$

where k_{id} is the intraparticle diffusion rate constant (mg/g $min^{1/2}$), C is the intercept (mg/g). Our experimental data, Fig. 19, revealed that the plot of q_t versus $t^{1/2}$ is multi-linear, An initial steep-sloped portion is followed by a linear portion to the intraparticle diffusion and a plateau to the equilibrium (Zeng *et al*., 2015). The initial steep-sloped portion is (from 2.24 to 5.48 $min^{1/2}$) is attributed to external surface adsorption or instantaneous adsorption, while the gentle-sloped portion (from 5.48 to 10.95 $min^{1/2}$) is attributed to gradual adsorption. The final stage was the equilibrium period, during which the intraparticle diffusion rate (from 10.95 to 15.49 $min^{1/2}$) slowed down and reached equilibrium. This reveals that the intraparticle diffusion is rate-controlled and leads to a plateau to the equilibrium. It should be noted that the intraparticle diffusion starts to slow down due to extremely low dye concentration in solution. The intraparticle diffusion rate was obtained from the slope of the gentle-sloped portion (Table 3). It is seen that the order of adsorption rates was the first stage ($k_{id,1}$) > second stage ($k_{id,2}$) > third stage ($k_{id,3}$). Therefore the changes of $k_{id,1}$, $k_{id,2}$, and $k_{id,3}$ could be attributed to the adsorption stages of the exterior surface, interior surface and equilibrium, respectively.

Table 3: Mechanism of CSB dye adsorption

Temp (K)	Intraparticle diffusion model									Film diffusion model	
	Part 1 (2.24-5.48)			Part 2 (5.48-10.95)			Part 3 (10.95-15.49)				
	$K_{id,1}$ (mg/g $min)^{0.5}$	C (mg/g)	R^2	$K_{id,2}$ (mg/g $min)^{0.5}$	C (mg/g)	R^2	$K_{id,3}$ (mg/g $min)^{0.5}$	C (mg/g)	R^2	Di (cm2/s)	R^2
304K	2.46	10.91	0.947	0.91	19.20	0.982	0.28	26.03	0.844	0.529	0.995
310K	2.16	13.54	0.927	0.86	20.49	0.969	0.24	27.27	0.650	1.029	0.995
318K	2.10	15.35	0.966	0.75	22.56	0.995	0.25	29.09	0.766	0.967	0.987
326K	2.00	16.84	0.935	0.81	23.26	0.963	0.25	29.41	0.710	0.994	0.995

The value of the intercept *C* in the second section provides information related to the thickness of the boundary layer. Larger intercepts suggest that boundary layer diffusion has a larger role as a rate-limiting step. The non-linearity of the plots indicates that the intraparticle diffusion cannot be accepted as the only rate controlling step for the adsorption of CSB onto $CuAl_2O_4$ nanoparticle surface. Thus, the overall rate of the adsorption process appears to be controlled by more than one-step. Our results agree well with other researchers (Mohammed *et al*., 2015; Xiang *et al*., 2017). This interpretation is consistent with the pseudo-second-order rate.

Evaluation of thermodynamic parameters:

The thermodynamic parameters ΔG (standard free energy), ΔH (enthalpy change) and ΔS° (entropy change) were calculated to determine the nature of the adsorption. The experimental data obtained at different temperatures were used to calculate the thermodynamic parameters by a plot of ln K_d versus 1/T (Fig. 20).by using the linear van't Hoff equation (Ridha *et al*., 2016).

$$\ln K_d = \frac{\Delta S}{R} - \frac{\Delta H}{RT} \quad (18)$$

where K_d represents the standard thermodynamic equilibrium constant as expressed by q_e/C_e (L/mg). The ΔG° (free energy change) was calculated by this equation:

$$\Delta G = - RT\ln K_d \quad (19)$$

where R is the gas constant of 8.314 J/mol K, T is the absolute temperature in K. and $K_d = q_e/C_e$ (L/mg) is the standard thermodynamic equilibrium constant.

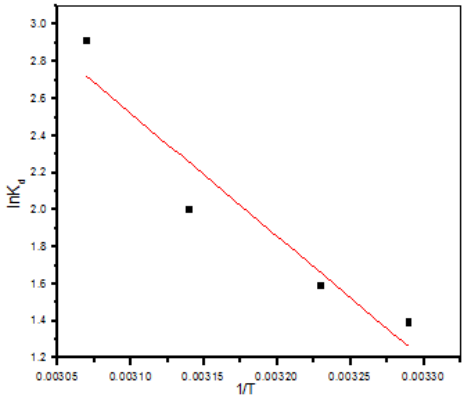

Fig. 20: Vant Hoff plot of CSB adsorption

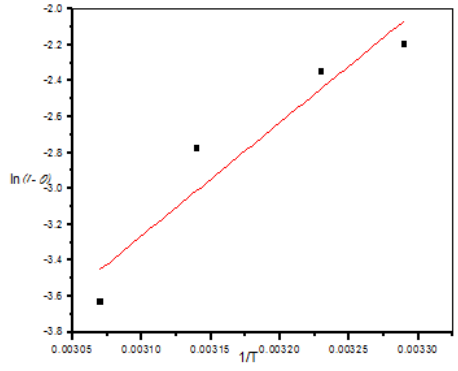

Fig. 21: Sticking probabillty of CSB adsorption

The negative ΔG values with increasing temperature indicates that adsorption of the CSB on the $CuAl_2O_4$ nanoparticle becomes favourable at a higher temperature (Table 4). The positive standard enthalpy change ΔH of 55.11kJ/mol suggests that the adsorption of CSB on the $CuAl_2O_4$ nanoparticle is an endothermic process. The positive standard entropy change of 192 J/mol K encourages the adsorption process. The increase in randomness at the solid-solution interface during the fixation of CSB on the active motifs of the $CuAl_2O_4$ nanoparticle is a consequence of loss of water molecules from the hydration shells of CSB dye. Our results agree well with other reports (Tiago *et al*., 2017; Hemant *et al*., 2017).

Table 4: Thermodynamic parameters of CSB dye adsorption

Temp.K	ΔG (kJ/mol)	ΔS (J/mol)	ΔH (KJ/mol)	R^2	Ea (KJ/mol)	S^*	R^2
304	-7.35	192	55.11		52.46	$1.23x10^{-10}$	0.86448
310	-4.10						
318	-5.29						
326	-7.89						

In order to further support the assertion that the adsorption is the predominant mechanism, the values of the apparent activation energy (E_a) and sticking probability (S*) were estimated from the experimental data (Table 4). They were calculated using a modified Arrhenius type equation related to surface coverage (Singh and Das, 2013) as expressed in equations (20,21):

$$\theta = 1 - \frac{C_e}{C_0} \quad (20)$$

$$S^* = (1 - \theta) \exp\left(-\frac{E_a}{RT}\right) \quad (21)$$

The sticking probability, S*, is a function of the adsorbate/adsorbent system under consideration and is dependent on the temperature of the system. The parameter S* indicates the measure of the potential of an adsorbate to remain on the adsorbent indefinitely. It can be explored as in (Fig.21). The effect of temperature on the sticking probability was evaluated throughout the temperature range from 304 to 326 K by calculating the surface coverage at the various temperatures. Table 3 indicated that the values of $S^* \leq 1$ for the $CuAl_2O_4$ nanoparticle, hence the sticking probability of the CSB dye onto the adsorbent system are very high.

Adsorption activation energy:

The magnitude of the apparent E_a gives an indication of the type of the adsorption process, physical or chemical. The physisorption process is readily reversible, equilibrium is attained rapidly and thus the energy requirements are small, ranging between 5 and 40 kJ/mol. The chemisorprtion mechanism is specific and involves stronger forces, and thus requires large activation energy ranging from 40 to 800 kJ/mol (Anirudhan and Radhakrishnan, 2008; Chakraborty *et al*., 2011). The high activation energy E_a of 52.46 kJ/mol, as calculated from the slope, reflects the chemical nature of the adsorption process.

Discussion on effect of molecular size and number of negative charges of dye on the adsorption process:

The adsorption isotherms well fitted the Langmuir model, indicating that the sorption of anionic dyes onto the $CuAl_2O_4$ nanoparticle was surface coverage by a mono-molecular layer and one $-SO_3^-$ group occupied one active site during the adsorption process. Also, it was reported that the molecular size and the electrical charge have an influence on electrostatic attraction (Zhao *et al*., 2014). Thus, the deviations in adsorption capacities for the studied dye could be explained by considering: (1) the number of negative charges of target dye; (2) molecular size of target dye.

For CSB, the number of negative charges per dye molecule was four (SO_3^- groups). Each one $-SO_3^-$ needs one cationic site on the adsorbent, therefore, four cationic sites are occupied by one molecule of CSB with four $-SO_3^-$ groups. On the other hand, the electrostatic repulsion could be formed between the adsorbed dye molecules and the free ones in bulk solution, which may well explain the lower sorption rate with increasing of contact time. Generally, the electrostatic repulsion became stronger as the increase in negative charge of dye molecules. Therefore, from the viewpoint of charge density, it is explainable that the q_{max} of CSB is low. Also, the lower q_{max} of CSB may be attributed to its much bigger molecular size shown in Fig. 1, because the much bigger size of the CSB molecule was unfavourable for its adsorption through electrostatic attraction. In summary, we can conclude that the charge density and the molecular size have significant influence on the adsorption of anionic dyes by $CuAl_2O_4$ nanoparticles.

Conclusion

$CuAl_2O_4$ nanoparticle was prepared by modifying Pechini method; the structure was confirmed by XRD and FTIR analyses. Adsorption of CSB dye process was described using four adsorption models, from this; the adsorption capacity in the value of 29.04 mg g^{-1} was obtained, associated to the chemisorption thermodynamically stable, the kinetics fitted to the pseudo-second order mechanism. The results of the present study showed mixed oxide Cu–Al is practical for the removal of CSB dye from aqueous water. The adsorption ability of dye remains high in a wide temperature range from 304 to 326 and the equilibrium data were described well by Langmuir isotherm model. The kinetic study revealed that the adsorption process followed the pseudo second-order kinetic model and the calculated thermodynamic parameters indicated that the adsorption process is spontaneous and endothermic in nature. The force that control adsorption of CSB onto mixed oxide Cu–Al is mainly electrostatic. Consequently, this adsorbent showed great potential for the treatment of coloured wastewaters.

References

Acharya, J., J.N. Sahu, C.R. Mohanty, B.C. Meikap, 2009. Chem. Eng. J., 149: 249-262.
Ahmad, R.B., G. Mehrorang, A. Arash, A.B. Ali, J. Ramin, 1017. Ultrasonics Sonochemistry, 34: 294-304.
Ahmed, A.A.A., Z.A. Talib, H.M.Z., Zakaria A., 2012. J. Alloy. Compd., 539: 154-160.
Agnès, B., O. Layaly, M. Rakotomalala, W. Mathias, T. Delphine, 1017. Journal of Magnetism and Magnetic Materials, 421: 59-64.
Arash, A., G. Mehrorang, H. Shaaker, G. Alireza, Al.D. Ebrahim, 2017. Ultrasonics Sonochemistry, 34: 1-12.
Alpat, S.K., Ö. Özbayrak, Ş. Alpat, H.A., 2008. J. Hazard Mater, 151: 213-220.
Anirudhan, T.S., P.G. Radhakrishnan, 2008. J. Chem. Thermodynamics, 40: 702-709.
Ariel, G., L. Enrique, A. Gisselle, 1016; Uriostegui-Ortegaa,Miguel A. Oliver-Tolentinoc, Esaú E. Rodríguez; Appl. Surf. Sci., 363: 372-380.
Banerjee, D., P. Bhowmick, D. Pahari, S. Santra, S. Sarkar, B. Das, K.K. Chattopadhyay, 2017. Physica E: Low-dimensional Systems and Nanostructures, 87: 68-76.
Boran, W., S. Lianghu, D. Xiaohu, C. Xiaoli, 2017. Chem.Eng. J., 307: 418-426.
Bouazizi, A., M.B., Karim A. Achiou, B. Ouammou, M. Calvo, J.I. Aaddane, A. Khiat, K. Alami, Y.S. 2017. Ceramics Inter., 43: 1479-1487.
Boyd, G.E., A.W. Adamson, L.S. Myers, 1949. J. Am. Chem. Soc., 69: 2836-2848.
Chakraborty, S., S. Chowdhury, P.D. Saha, 2011. Carbohydrate Polym, 86: 1533-1541.
Chunsheng, L., Z.u. Xiaofeng, Z. Bicheng, J. Chuanjia, L. Yao, Y. Jiaguo, 2017. J. Hazard. Mater., 321: 801-811.
Dordio, A.V., S. Miranda, R.J.P. Prates, A.J. Palace Carvalho, 2017. J. Hazard. Mater., 323: 575-583.
Dubinin, M.M., L.V. Radushkevich, 1947. Chem. Zentr, 875-889.
Duran, C., D. Ozdes, A. Gundogdu, H.B. Senturk, 2011. J. Chem. Eng. Data, 56: 2136-2147.
Fan, Y., J. Qun, Z. Moran, Z. Lulu, Z.g.Ying, 2017. Sci. Total Environm., 577: 54-60.
Freundlich, H.M.F., 1906. Über die adsorption in lösungen. Z. Phys. Chem. (Leipzig) 57A: 385-470.
Gao, H., T.K.S. Zhao, Y. Qian, X. Cheng, W. Wu, X. Wang, L. Zheng, 2013. J Hazard Mater, 261: 83-90.
Gautam, R.K., A. Mudhoo, M.C. Chattopadhyaya, 2013. J. Environ. Chem. Eng., 1: 1283-1291.
Hemant, S., C. Garima, K. Arinjay, S.K.S. Jain, 2017; J. Environm. Chem. Eng., 5: 122-135.
Ho, Y.S., G. McKay, 1999. Process. Biochem., 34: 451-465.
Jain, M., V.K. Garg, K. Kadivelu, 2010. J Environ Manag, 91: 949-957.
Lagergren, S.,1898. Handlingar, 24(4): 1-39.
Langmuir, I., 1918. J. Am. Chem. Soc., 40: 1361-1403.
Lin, W., G. Haoshuang, H. Jian, Z. Tingting, Z. Xuewen, X. Chuan, L. Hui, Z.g. Xianghui, L. Yuebin, 2017. J. Alloys and Compounds, 695: 599-606.
Lu, Y.g., W. Fazhou, H. Amer, E.M. Donald, L. Peng, H. Shuguang, 2017. Appl. Surf. Sci., 392: 687-696.
Ma, J., F. Yu, L. Zhou, L. Jin, M. Yang, J. Luan, Y. Tang, H. Fan, Z. Yuan, J. Chen, 2012. Appl Mater Interf., 4: 5749-5760.
Mayur, B.K., R.W. Tatoba, M.P. Swapnil, J. Byong-Hun, P.G. Sanjay, 2017. Chem. Eng. J., 307: 1026-1036.
Mei-Yu, G., X. Dong-Mei, S. Yu-Fei, G. Ying, 2013. Sensors and Actuators B: Chemical., 188: 1148-1154.
Mena, E., A.R., E.M. Rodríguez, F.J. Beltrán, 2017. Catalysis Today, 280(1): 74-79.
Mohammed, K., T. Mohamed, M. Rachida, N. Noureddine, B. Bachir, A. Abdeltif, 2015. J.Environm. Chem. Eng., 3: 548-559.
Muhammad, S., T. Hajira, K. Jawariya, H. Uzma, S. Atika, 2017. Ultrasonics Sonochemistry, 34: 600-608.
Nishimura, H., G. Nelson, W. Rosenblum, 1989. Microcirc Endothelium Lymphatics, 5(6): 435-40.
Reichenberg, D., 1953. J. Am. Chem. Soc., 75: 589-597.
Ridha, L., C. Khaled, A.D. Mohamed, B.H.A. Abdessalem, H. Amor, 2016. Adv. Powd. Tech., 27: 232-237.

Robati, D., M. Rajabi, O. Moradi, F. Najafi, I. Tyagi, S. Agarwal, V.K. Gupta, 2015. J. Mol. Liq., 214: 259-263.
Roohan, R., N. Yasaman, 2017. J. Magnetism and Magnetic Mater., 422: 128-140.
Roosta, M.M.G., A. Daneshfar, R. Sahraei, 2014. Spectrochim. Acta, Part A, 122: 223-231.
Seliem, M.K., S. Komarneni, R. Mostafa, 2016. Microporous and Mesoporous Mater., 224: 51-57.
Silva, A.A.D., A.D.S. Gonçalves, M.R. Davolos, 2009. J. Sol-Gel Sci. Technol., 49: 101-105.
Shisuo, F., T. Jie, W. Yi, L. Hui, Z. Hao, T. Jun, W. Zhen, L. Xuede, 2016. J. Molecular Liquids, 220: 432-441.
Shuheng, Y., Z. Jiajun, S. Dekui, X. Rui, G. Sai, Z. Ming, L. Junyu, 2016. J. Colloid and Interf. Sci., 463: 118-127.
Sílvia, C.R.S., A.R.B. Rui, 2016. J. Environm.Chem.Eng., 4: 1473-1483.
Singh, B., S.K. Das, 2013. Colloids and Surf. B: Biointer., 107: 97-106.
Sneha, C., U. Himani, Y. Mohit, B. Nupur, S. Nahar, 2017. Ecotoxicology and Environm. Safety, 135: 68-74.
Somaye, M., S. Razieh, J. Hamedreza, G. Maryam, T. Inderjeet, A. Shilpi, K.G. Vinod, 2016. J. Molecular Liquids, 215: 144-153.
Somayeh, D., G. Mehrorang, A. Arash, Z. Fahimeh, W. Shaobin, 2017. Ultrasonics Sonochemistry, 34: 343-353.
Temkin, I.M., V. Pyzhev, 1940. Acta Physiochem. SSR 12: 217-222.
Thines, K.R., E.C. Abdullah, N.M. Mubarak, M. Ruthiraan, 2017. Renewable and Sustainable Energy Reviews, 67: 257-276.
Tiago, D.O., G. Régis, T. Thomas, L.M. Claude, M. Fabrice, T. Vinicius, G. Marcelo, B. Mohammed, 2017. J. Hazard. Mater., 323: 558-566.
Tomić, N.M., Z.D. Dohčević-Mitrović, N.M. Paunović, D.Ž. Mijin, N.D. Radić, B.V. Grbić, S.M. Aškrabić, B.M. Babić, D.V. Bajuk-Bogdanović, 2014. Langmuir, 30: 11582-11590.
Weber, J.W.J., J.C. Morris, 1963. J. Sanit. Eng. Div. ASCE, 89(SA2):31-59.
Wei, Z., Z. Wenpeng, C. Zilin, 2017. Appl. Surf. Sci., 392: 153-161.
Xiaoyun, S., Z. Jun, Z.g Shaohua, L. Wei, C. Qiang, C. Bingqiang, 2012. Mater. Res. Bull., 47: 4305-4310.
Xin, H(a)., G. Baoyu, S. Yangyang, Y. Qinyan, W. Yan, L. Qian, X. Xing, 2017. Sep. and Pur. Tech., 173: 209-217.
Xin, S(b)., W. Rui, Z. Weifeng, S. Shudong, Z. Changsheng, 2017. 2nd- J. Colloid and Interf. Sci., 485: 39-50.
Xin, Z(c)., Z.g. Liangmiao, X. Pan, M. Wenjing, Q. Na, L. Wencong, 2015. Microporous and Mesoporous Materials., 201: 91-98.
Xiang, H., Z. Hua, S. Zhirong, 2017. Appl. Surf. Sci., 392: 332-341.
Xiaoming, H., P. Min, 2016. J. Molecular Liquids, 215: 410-416.
Ying-Lung, H., L. Yung-Chung, C. Chieh-Lun, Y. Wan-Ju, N. Dillirani, L. Chih-Hsi, L. Yi-Heng, C. Jo-Shu, 2017. Biochem. Eng. J.l, 117: 48-56.
Yue, C., L. Xiang-Yang, C.g. Tai-Shung, W. Martin, St. Claudia, M. Christian, 2016. Water Res., 91: 104-114.
Yunchuan, Q., Y. Meiling, X. Wenhui, H. Sha, M. Yi, 2017. J. Colloid and Interf. Sci.e, 486: 84-96.
Zeng, G., Y. Liu, L. Tang, G. Yang, Y. Pang, Y. Zhang, Y. Zhou, Z. Li, M. Li, M. Lai, X. He, Y. He, 2015. Chem. Eng. J., 259: 153-160.
Zhao, X., J. Huang, B. Wang, Q. Bi, L. Dong, X.L., 2014. Appl Surf Sci., 292: 576-582.
Zhenzhen, H., C. Guiqiu, Z. Guangming, G.o. Zhi, H. Kai, H. Liang, W. Jing, Z. Lihua, Z. Yuan, S. Zhongxian, 2017. J. Hazard. Mater., 321: 37-46.
Zhijie, L., Z. Zhiwei, S. Tianyi, S. Wenxin, C. Fuyi, 2017. J. Colloid and Interf. Sci., 485: 192-200.